ACS Photonics

Letter

pubs.acs.org/journal/apchd5

Strong Near-Field Coupling of Plasmonic Resonators Embedded in Si Nanowires

Dmitriy S. Boyuk, Li-Wei Chou, and Michael A. Filler*

School of Chemical & Biomolecular Engineering, Georgia Institute of Technology, Atlanta, Georgia 30332, United States

Supporting Information

ABSTRACT: The strength of localized surface plasmon resonance (LSPR) near-field interactions scales in a well-known, nearly universal manner. Here, we show that embedding resonators in an anisotropic dielectric with a large permittivity can substantially increase coupling strength. We experimentally demonstrate this effect with Si nanowires containing two phosphorus-doped segments. The near-field decay length scaling factor is extracted from *in situ* infrared spectral response measurements using the "plasmon ruler" equation and found to be ca. 4−5 times larger than for the same resonators in isotropic vacuum or Si. Discrete dipole approximation calculations support the observed coupling behavior for nanowires and show how it is affected by the resonator geometry, carrier density, and embedding material (Si, Ge, GaAs, etc.). Our findings demonstrate that equivalent near-field interactions are achievable with a smaller total volume and/or at increased resonator spacing, offering new opportunities to engineer plasmon-based chemical sensors, catalysts, and waveguides.

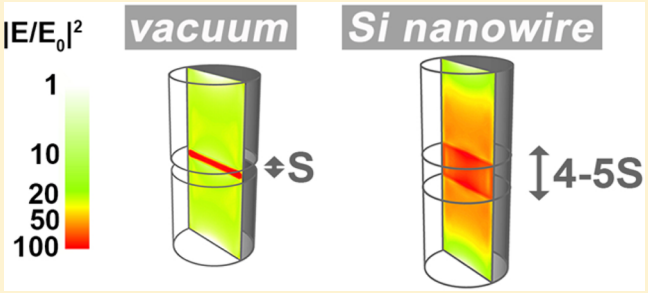

KEYWORDS: *silicon nanowire, doping, surface plasmon resonance, coupling*

Resonant surface charge density oscillations supported by small metallic particles, known as localized surface plasmon resonances (LSPRs), provide a route to enhance the sensitivity of chemical detectors,[1,2] activity of heterogeneous catalysts,[3,4] and compactness of waveguides.[5,6] These opportunities emerge from two key properties of the LSPR: (i) deep subwavelength photon confinement and (ii) enhanced local electric fields.[7] The near-field coupling between closely spaced resonators enables further light focusing, stronger local electric fields, and energy transport via dipolar coupling.[8−10] Near-field coupling interactions are a strong function of resonator size and separation,[11−13] with larger resonators and/or shorter inter-resonator distances resulting in stronger coupling. However, these are conflicting requirements for many applications: large electric fields are often desired in the smallest possible footprint. Obtaining the largest local electric fields also necessitates that neighboring resonators be separated by nanometer, or even subnanometer, gaps, and this degree of precision continues to be challenging in high-volume manufacturing environments.

The near-field coupling strength of dipolar LSPRs can be determined (in the quasi-static limit) by analyzing far-field spectral response measurements with the so-called "plasmon ruler" equation,[12−14] which describes the relationship between absorption peak position and resonator spacing:

$$\frac{\omega - \omega_0}{\omega_0} = A \exp\left[\frac{-S/L}{\tau}\right] \quad (1)$$

where ω_0 is the peak absorption frequency for an isolated resonator of length L, and ω is the peak absorption frequency for two resonators of length L separated by a distance S. A is a dimensionless constant of proportionality. τ is known as the decay length scaling factor, a dimensionless parameter that describes the rate at which the electric field decays away from the surface of each resonator. Larger values of τ indicate longer electric field decay lengths and stronger near-field coupling interactions. Previous work supports the validity of eq 1 for coupled dipolar LSPRs in purely isotropic (e.g., nanoparticles dispersed in solution)[15−19] as well as anisotropic (e.g., patterned metal particles on a substrate) dielectric environments.[20−23] Most importantly, τ is found to be nearly independent of nanoparticle size, shape, metal, and surrounding dielectric.[14,23−27] Closely spaced sphere, disk, and pyramid dimers composed of either Au or Ag all exhibit τ values in the 0.2−0.3 range. Hence, the LSPR near-field decays over a distance about one-fifth to one-third of the resonator size.[23,27]

Doped semiconductors are promising plasmonic materials for applications in the mid- to near-infrared spectral regime.[28−30] We previously demonstrated mid-infrared LSPRs supported by fully and partially doped Si nanowires synthesized by the bottom-up vapor−liquid−solid (VLS) technique.[31−33] The programmability of the axial dopant profile presents unique opportunities to both manipulate and understand near-field coupling interactions in doped-semiconductor nanostruc-

Received: October 10, 2015
Published: January 25, 2016

DOI: 10.1021/acsphotonics.5b00581
ACS Photonics 2016, 3, 184−189

tures. Here, we combine *in situ* infrared spectroscopy and discrete dipole approximation (DDA) calculations to characterize the coupling of doped Si resonators embedded along the length of Si nanowires. We show, relative to previous reports, a ca. 4−5 times enhancement in LSPR near-field decay length. This behavior emerges from a synergy between the nanowire's structural anisotropy and intrinsic Si's large permittivity in the infrared.

Figure 1a displays representative scanning electron microscope (SEM) images of epitaxial Si nanowires containing one

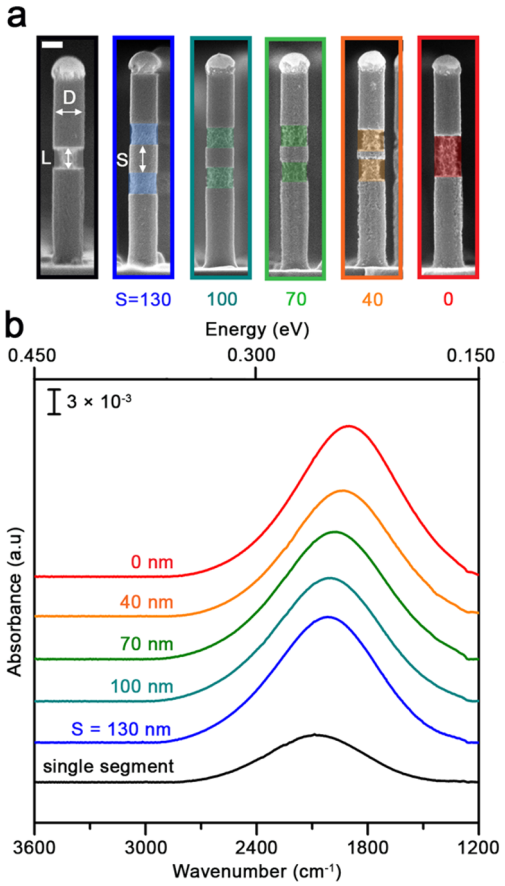

Figure 1. Red-shift of absorption frequency for coupled LSPRs in Si nanowires. (a) Side view SEM images of representative Si nanowires following a buffered oxide etch treatment to determine doped segment geometry (AR = 0.8) and separation distance (130, 100, 70, 40, and 0 nm). Scale bar: 100 nm. (b) Spectral response measurements of the longitudinal LSPR mode for arrays of the Si nanowires shown in (a).

or two phosphorus-doped segments. These images are taken *following* a buffered oxide etch (BOE) treatment that reveals resonator placement and dimensions. All resonators exhibit a length of 100 nm, which corresponds to an aspect ratio (AR) of 0.8. Figure 1b displays *in situ* spectral response measurements, acquired immediately after growth and *before* BOE treatment, for the nanowire arrays in Figure 1a. As described in the Methods, these measurements are sensitive to LSPRs with dipoles oriented along the nanowire length (i.e., longitudinally). Si nanowires containing a single doped segment exhibit a single LSPR absorption feature centered at 2088 cm^{-1} (ω_0), consistent with a carrier density of 2.7×10^{20} cm^{-3}. Similar to previous reports[12−14] and as expected from dipole−dipole coupling theory,[11,24] the absorption peak position for neighboring resonators (ω) red-shifts with decreasing resonator separation distance (S).

We use the plasmon ruler equation, as shown in Figure 2, to determine the decay length scaling factor (τ) for our embedded

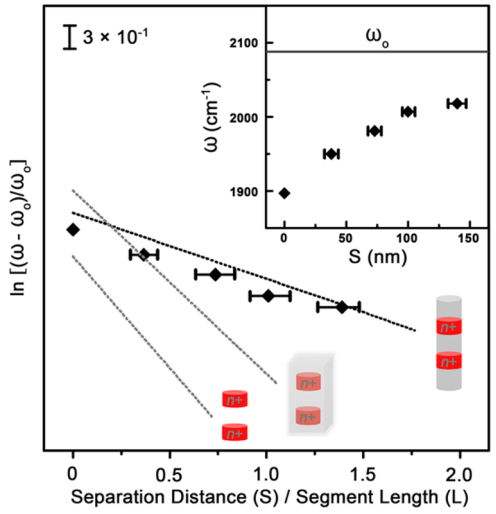

Figure 2. Determination of decay length scaling factor. Experimental absorption peak frequencies and doped Si resonator separation distances are extracted from Figure 1, as shown in the inset, and plotted according to a linearized form of eq 1. τ can be extracted from the slope of these points. Error bars are for one standard deviation. Linear fits to calculated absorption peak frequencies (see spectra in Figures S1 and S2) for doped Si segments embedded in nanowires, isotropic vacuum, and isotropic Si are shown as dotted lines.

resonators. Equation 1 is linearized, and the ω values from Figure 1 are plotted accordingly. We find that the value of τ, which can be extracted from the slope, is 1.4 for this resonator geometry and carrier density. Consistent with these data, calculations yield an absorption peak red shift as resonator spacing decreases (Supporting Information, Figure S1) and a τ value of 1.7. However, as seen in Figure 2, LSPRs supported by doped Si resonators placed in an isotropic dielectric that is either vacuum or intrinsic Si exhibit τ values of ∼0.4 (Supporting Information, Figure S1). These values are in line with published results for noble metals[14,27] and $Cu_{2-x}S$ nanodisks.[35] The τ value for coupled resonators embedded in isotropic Si is determined from one of two dipolar resonances (Supporting Information, Figure S2). The motivation for, and validity of, this approach is fully described in the Supporting Information (Isotropic Si Dielectric Environments and Figures S3−S5).

Strikingly, the nanowire structure enables an approximately 4−5-fold increase in near-field decay length. For nanowires, the structural anisotropy and large permittivity of intrinsic Si (n = 3.4) lead to a strong concentration of the electric field in the volume between adjacent resonators (Supporting Information, Figure S6a). This behavior greatly enhances the near-field coupling strength. For equivalent resonators placed in an isotropic vacuum (Supporting Information, Figure S6b) or isotropic Si (Supporting Information, Figure S6c), the largest field enhancements occur near the resonator corners, which prevents the same degree of coupling. In both the nanowire and isotropic Si cases, the resonators are axially separated by a high permittivity medium (i.e., Si). However, in the latter case, the presence of intrinsic Si in the radial direction results in an

DOI: 10.1021/acsphotonics.5b00581
ACS Photonics 2016, 3, 184−189

image dipole that counteracts and defocuses the field.[31,36] As shown in Figure 3, and expected from the preceding discussion,

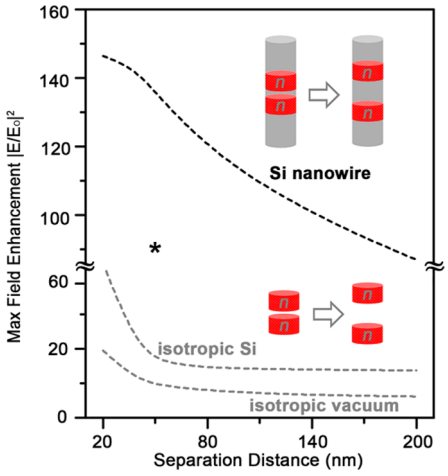

Figure 3. Maximum field enhancement for coupled Si resonators as a function of resonator separation in a Si nanowire, isotropic vacuum, and isotropic Si. The corresponding electric field enhancement maps are shown in Figure S6. The star at a separation distance of 60 nm indicates the approximate field enhancement obtained in the vacuum cut-out of the nanowire shown in Figure S7. To match the dimensions of nanowires obtained experimentally, calculations are performed for cylindrical nanowires with a diameter and length of 130 and 950 nm, respectively.

resonators embedded in nanowires yield local fields stronger than resonators in an isotropic vacuum *for the same spacing*. While the maximum enhancement for isotropic vacuum asymptotes at ~10 for resonator separations above 50 nm, resonators embedded in a Si nanowire separated by a distance of 200 nm still support enhancements near 90.

DDA allows us to explore the role of nanowire structure on near-field interactions. We determine τ values for doped Si resonators embedded in GaAs (n = 3.2), Si (3.4), and Ge (4.1) nanowires, or an isotropic vacuum, as a function of the resonator aspect ratio and carrier density. We choose these materials since the VLS growth of nanowires is possible for each.[37,38] Figure 4a shows that small AR resonators yield the largest decay length scaling factors. This behavior is expected from the plasmon ruler equation (i.e., as L decreases at constant S, τ must increase) and has been observed for Au nanorods.[26] Resonators embedded in nanowires amplify this effect due to their anisotropic structure. Figure 4b shows that increasing carrier density yields larger τ values. Coupling increases because the plasma frequency (ω_p), and therefore the polarizability, of each resonator increases with carrier density.[39] Figure 4a and b also show that τ increases with the permittivity of the embedding nanowire material.[8,25]

The benefits of enhanced decay length scaling factors become clear when considering the needs of devices that leverage near-field plasmon interactions such as waveguides, chemical sensors, and photodetectors. Maximizing the interaction strength, and thereby the distance over which energy can be transported, is critical for subwavelength waveguides.[40,41] More specifically, ohmic losses demand as few plasmonic resonators as possible per unit waveguide length. A 4−5 times larger near-field decay length, as observed here, allows a 4−5 times increase in inter-nanoparticle distance and, therefore, a concomitant increase in energy transport distance. Calculations

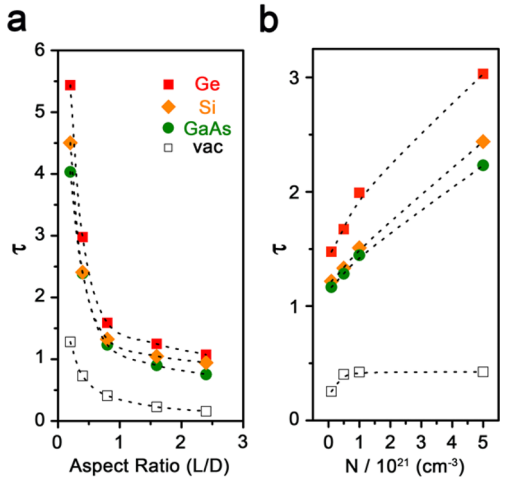

Figure 4. Calculations of near-field decay length scaling factor for nanowires as a function of resonator (a) aspect ratio (for $n = 3 \times 10^{20}$ cm^{-3}) and (b) carrier concentration (for AR = 0.8). Red squares, orange diamonds, and green circles represent doped Si resonators embedded in Ge, Si, and GaAs nanowires, respectively. Open black squares represent equivalent doped Si resonators in an isotropic vacuum. Calculations are performed for cylindrical nanowires with a diameter and length of 150 and 1500 nm, respectively.

are currently under way in our laboratory to quantitatively understand and predict the performance (e.g., propagation length) of subwavelength-doped nanowire waveguides.

Our results also show how anisotropic structures, such as nanowires, can improve the sensitivity and reduce the physical size of plasmon-based chemical sensors and photodetectors. As discussed above (Figure 3), nanowires offer higher local electric fields, and therefore sensitivities, for the same resonator spacing. Alternatively, anisotropy can relax the precision required of the fabrication process (e.g., lithography and etching),[10,18] since it provides the same local electric field at larger resonator spacing. For example, as shown in Figure 5a, resonators of the same geometry (AR = 1.6) separated by 100 nm in a Si nanowire and 20 nm in an isotropic vacuum yield the same maximum local field enhancement. Increasing resonator length can also strengthen local electric fields, but this increases overall device size. Figure 5b shows that doped Si resonators separated by a segment of intrinsic Si achieve field enhancements equivalent to that of 60% larger resonators in an isotropic vacuum.

It should be noted that optically active materials must be placed in, or molecules must access, the region of highest electric field (i.e., inside the intrinsic Si separating the doped segments) for photon and chemical detectors, respectively. VLS is well equipped to insert thin layers of other photoactive semiconductors,[42−44] and recent work shows a new route to embed silicides.[45] Selective etching can enable the small radial cut-outs necessary for mass transport into and out of the high-field region.[46] The introduction of a cut-out consisting of a low-permittivity medium (e.g., gas) will reduce the magnitude of the field enhancement, as seen in Figure S7. Nonetheless, for this structure, as indicated by the star in Figure 3, the maximum electric fields located in the cut-outs exceed those for the same resonators embedded in an isotropic medium by ~8 times.

The small differences in the decay length scaling factors determined from experiment and simulation (Figure 2) are also worthy of discussion. We attribute this behavior to the

DOI: 10.1021/acsphotonics.5b00581
ACS Photonics 2016, 3, 184−189

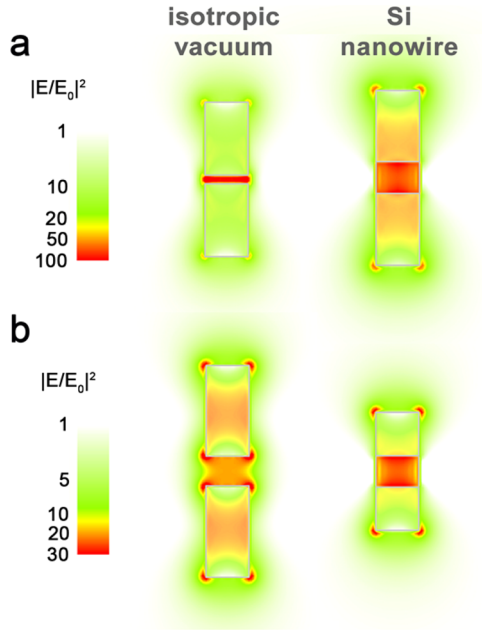

Figure 5. Advantages of structural anisotropy. Calculated electric field enhancement maps for the longitudinal mode of cylindrical doped Si resonators each with a carrier concentration of 2.7×10^{20} cm^{-3}. (a) Equivalent field enhancement magnitudes (~100) are calculated between two resonators with AR = 1.6 separated by 20 nm of vacuum and 100 nm of Si. (b) Equivalent field enhancement magnitudes (~30) are achieved between two resonators of AR = 1.6 (length = 240 nm) separated by vacuum and AR = 1.0 (length = 150 nm) separated by Si.

nonidealities of semiconductor nanowire growth via the vapor−liquid−solid technique. A small amount of sidewall deposition (<10 nm) cannot be ruled out and will produce an image dipole that damps the LSPR.[31,36] This behavior reduces near-field coupling strength, as seen for coupled resonators embedded in Si nanowires with 5 and 10 nm intrinsic Si shells (Supporting Information, Figure S8). Notably, VLS growth likely yields a shell whose thickness depends on axial position (due to the concurrent elongation of the nanowire) and/or contains additional carriers (due to PCl_3 decomposition on the sidewall). Nonetheless, careful control of nanowire structure will be crucial to obtain the highest near-field coupling strengths.

We have experimentally shown that the near-field decay length scaling factor determined using the plasmon ruler equation for doped Si resonators embedded in Si nanowires exceeds the well-known "universal" value for noble metals in the UV/visible by 4−5 times. The anisotropic structure of semiconductor nanowires and large permittivity of intrinsic Si in the infrared underlies this behavior. Our findings offer several new design options for plasmon-based detectors, catalysts, and waveguides. In addition, our results indicate that use of the plasmon ruler to measure nanoscale distance, without ensuring that the dielectric environment is truly isotropic, may lead to experimental errors.

METHODS

A Si (111) substrate (El-Cat, FZ, 15−30 Ω-cm, double side polished) is cleaned by a 5 min immersion in 10% HF (J.T. Baker) and subsequently rinsed in deionized water prior to insertion into an ultra-high-vacuum (UHV) chamber.[47] The substrate is degassed at 700 °C for 1 h and then flash-annealed at 1200 °C for 30 s under vacuum. After cooling the substrate at a rate of less than 2 °C/s, a thin film of Au (ESPI Metals, 99.999%) is deposited at a rate of ~1 Å/min using a high-temperature effusion cell (SVT Associates). Si nanowires containing one or two doped segments, each 100 nm in length, are then fabricated using the VLS technique in a two-step process. In the first step, Au film breakup and nanowire nucleation is accomplished by ramping to and holding the substrate temperature at 620 °C while maintaining Si_2H_6 (Voltaix, 99.998%) at a pressure of 4×10^{-5} Torr for 2 min. Nanowire areal densities and mean diameters of ~1 nanowire/μm^2 and 130 nm are obtained using this procedure. In the second step, the substrate temperature is lowered to 470 °C with the Si_2H_6 partial pressure fixed at 4×10^{-5} Torr. These conditions result in a nanowire growth rate of ~4 nm/min. Each phosphorus-doped segment is encoded by introducing PCl_3 (Strem Chemicals, 99.999%) at a partial pressure of 3×10^{-6} Torr for 25 min. PCl_3 does not strongly impact nanowire growth rate.[48] Precursor partial pressures are not corrected for ion gauge sensitivity.

We measure the far-field absorption spectra of as-grown nanowire arrays at room temperature immediately following growth under vacuum using *in situ* infrared spectroscopy (Bruker, Vertex 70).[32−34] Unpolarized light from a standard SiC globar source is combined with a KBr beam splitter and a liquid nitrogen-cooled HgCdTe detector to collect spectra between 700 and 3600 cm^{-1}. All spectra are recorded with a resolution of 4 cm^{-1}, at an incidence angle of 58° to access the longitudinal LSPR mode, and are baseline corrected using a concave rubberband method. After synthesis and spectral response measurement, nanowire arrays are removed from the UHV system and treated with BOE (J.T. Baker 7:1) solution to reveal doped segment geometry. Nanowire morphology before and after BOE treatment is examined using a Zeiss Ultra 60 field-emission scanning electron microscope.

The spectral responses of the doped Si nanowires are simulated within the discrete dipole approximation using the FLTRCD method available in the DDSCAT 7.3 code.[34] Nanowires are modeled as ideal cylinders with overall and doped segment dimensions matching experiment, and the incident electric field is polarized along the nanowire axis (i.e., longitudinally). Single nanowire calculations are appropriate for this investigation since array areal densities are sufficiently low (~1 nanowire/μm^2) such that inter-nanowire LSPR interactions can be neglected.[31] The refractive indices (n) and extinction coefficients (k) of undoped and doped Si segments are obtained from Palik[49] and an extended Drude model,[33] respectively. Unless otherwise noted, a grid spacing of 10 nm is used in all calculations and a conjugate gradient iteration is completed until achieving an error tolerance below 10^{-5}.

ASSOCIATED CONTENT

Supporting Information

The Supporting Information is available free of charge on the ACS Publications website at DOI: 10.1021/acsphotonics.5b00581.

Additional details (PDF)

AUTHOR INFORMATION

Corresponding Author

*E-mail: mfiller@gatech.edu.

DOI: 10.1021/acsphotonics.5b00581
ACS Photonics 2016, 3, 184−189

Notes

The authors declare no competing financial interest.

■ ACKNOWLEDGMENTS

The authors gratefully acknowledge support from the National Science Foundation (nos. 1069138 and 1510934) and the Camille and Henry Dreyfus Postdoctoral Program in Environmental Chemistry.

■ REFERENCES

(1) Mayer, K. M.; Hafner, J. H. Localized Surface Plasmon Resonance Sensors. *Chem. Rev.* **2011**, *111*, 3828−3857.
(2) Baldassarre, L.; Sakat, E.; Frigerio, J.; Samarelli, A.; Gallacher, K.; Calandrini, E.; Isella, G.; Paul, D. J.; Ortolani, M.; Biagioni, P. Midinfrared Plasmon-Enhanced Spectroscopy with Germanium Antennas on Silicon Substrates. *Nano Lett.* **2015**, *15*, 7225−7231.
(3) Linic, S.; Aslam, U.; Boerigter, C.; Morabito, M. Photochemical Transformations on Plasmonic Metal Nanoparticles. *Nat. Mater.* **2015**, *14*, 744−744.
(4) Mukherjee, S.; Zhou, L. A.; Goodman, A. M.; Large, N.; Ayala-Orozco, C.; Zhang, Y.; Nordlander, P.; Halas, N. J. Hot-Electron-Induced Dissociation of H_2 on Gold Nanoparticles Supported on SiO_2. *J. Am. Chem. Soc.* **2014**, *136*, 64−67.
(5) Maier, S. A.; Atwater, H. A. Plasmonics: Localization and Guiding of Electromagnetic Energy in Metal/Dielectric Structures. *J. Appl. Phys.* **2005**, *98*, 011101.
(6) Apuzzo, A.; Fevrier, M.; Salas-Montiel, R.; Bruyant, A.; Chelnokov, A.; Lerondel, G.; Dagens, B.; Blaize, S. Observation of Near-Field Dipolar Interactions Involved in a Metal Nanoparticle Chain Waveguide. *Nano Lett.* **2013**, *13*, 1000−1006.
(7) Gramotnev, D. K.; Bozhevolnyi, S. I. Plasmonics Beyond the Diffraction Limit. *Nat. Photonics* **2010**, *4*, 83−91.
(8) Schuller, J. A.; Barnard, E. S.; Cai, W. S.; Jun, Y. C.; White, J. S.; Brongersma, M. L. Plasmonics for Extreme Light Concentration and Manipulation. *Nat. Mater.* **2010**, *9*, 193−204.
(9) Alu, A.; Belov, P. A.; Engheta, N. Coupling and Guided Propagation Along Parallel Chains of Plasmonic Nanoparticles. *New J. Phys.* **2011**, *13*, 033026.
(10) Mayer, K. M.; Hafner, J. H. Localized Surface Plasmon Resonance Sensors. *Chem. Rev.* **2011**, *111*, 3828−3857.
(11) Nordlander, P.; Oubre, C.; Prodan, E.; Li, K.; Stockman, M. I. Plasmon Hybridizaton in Nanoparticle Dimers. *Nano Lett.* **2004**, *4*, 899−903.
(12) Rechberger, W.; Hohenau, A.; Leitner, A.; Krenn, J. R.; Lamprecht, B.; Aussenegg, F. R. Optical Properties of Two Interacting Gold Nanoparticles. *Opt. Commun.* **2003**, *220*, 137−141.
(13) Su, K. H.; Wei, Q. H.; Zhang, X.; Mock, J. J.; Smith, D. R.; Schultz, S. Interparticle Coupling Effects on Plasmon Resonances of Nanogold Particles. *Nano Lett.* **2003**, *3*, 1087−1090.
(14) Gunnarsson, L.; Rindzevicius, T.; Prikulis, J.; Kasemo, B.; Kall, M.; Zou, S. L.; Schatz, G. C. Confined Plasmons in Nanofabricated Single Silver Particle Pairs: Experimental Observations of Strong Interparticle Interactions. *J. Phys. Chem. B* **2005**, *109*, 1079−1087.
(15) Underwood, S.; Mulvaney, P. Effect of the Solution Refractive-Index on the Color of Gold Colloids. *Langmuir* **1994**, *10*, 3427−3430.
(16) Jensen, T. R.; Duval, M. L.; Kelly, K. L.; Lazarides, A. A.; Schatz, G. C.; Van Duyne, R. P. Nanosphere Lithography: Effect of the External Dielectric Medium on the Surface Plasmon Resonance Spectrum of a Periodic Array of Sliver Nanoparticles. *J. Phys. Chem. B* **1999**, *103*, 9846−9853.
(17) Prodan, E.; Lee, A.; Nordlander, P. The Effect of a Dielectric Core and Embedding Medium on the Polarizability of Metallic Nanoshells. *Chem. Phys. Lett.* **2002**, *360*, 325−332.
(18) Lee, K. S.; El-Sayed, M. A. Gold and Silver Nanoparticles in Sensing and Imaging: Sensitivity of Plasmon Response to Size, Shape, and Metal Composition. *J. Phys. Chem. B* **2006**, *110*, 19220−19225.
(19) Jain, P. K.; El-Sayed, M. A. Noble Metal Nanoparticle Pairs: Effect of Medium for Enhanced Nanosensing. *Nano Lett.* **2008**, *8*, 4347−4352.
(20) Sonnichsen, C.; Reinhard, B. M.; Liphardt, J.; Alivisatos, A. P. A Molecular Ruler Based on Plasmon Coupling of Single Gold and Silver Nanoparticles. *Nat. Biotechnol.* **2005**, *23*, 741−745.
(21) Funston, A. M.; Novo, C.; Davis, T. J.; Mulvaney, P. Plasmon Coupling of Gold Nanorods at Short Distances and in Different Geometries. *Nano Lett.* **2009**, *9*, 1651−1658.
(22) Liu, N.; Hentschel, M.; Weiss, T.; Alivisatos, A. P.; Giessen, H. Three-Dimensional Plasmon Rulers. *Science* **2011**, *332*, 1407−1410.
(23) Jain, P. K.; Huang, W. Y.; El-Sayed, M. A. On the Universal Scaling Behavior of the Distance Decay of Plasmon Coupling in Metal Nanoparticle Pairs: A Plasmon Ruler Equation. *Nano Lett.* **2007**, *7*, 2080−2088.
(24) Willingham, B.; Brandl, D. W.; Nordlander, P. Plasmon Hybridization in Nanorod Dimers. *Appl. Phys. B: Lasers Opt.* **2008**, *93*, 209−216.
(25) Prodan, E.; Radloff, C.; Halas, N. J.; Nordlander, P. A Hybridization Model for the Plasmon Response of Complex Nanostructures. *Science* **2003**, *302*, 419−422.
(26) Jain, P. K.; Eustis, S.; El-Sayed, M. A. Plasmon Coupling in Nanorod Assemblies: Optical Absorption, Discrete Dipole Approximation Simulation, and Exciton-Coupling Model. *J. Phys. Chem. B* **2006**, *110*, 18243−18253.
(27) Tabor, C.; Murali, R.; Mahmoud, M.; El-Sayed, M. A. On the Use of Plasmonic Nanoparticle Pairs as a Plasmon Ruler: The Dependence of the near-Field Dipole Plasmon Coupling on Nanoparticle Size and Shape. *J. Phys. Chem. A* **2009**, *113*, 1946−1953.
(28) Naik, G. V.; Shalaev, V. M.; Boltasseva, A. Alternative Plasmonic Materials: Beyond Gold and Silver. *Adv. Mater.* **2013**, *25*, 3264−3294.
(29) Liu, X.; Swihart, M. T. Heavily-Doped Colloidal Semiconductor and Metal Oxide Nanocrystals: An Emerging New Class of Plasmonic Nanomaterials. *Chem. Soc. Rev.* **2014**, *43*, 3908−3920.
(30) Zhong, Y. J.; Malagari, S. D.; Hamilton, T.; Wasserman, D. Review of Mid-Infrared Plasmonic Materials. *J. Nanophotonics* **2015**, *9*, 093791.
(31) Chou, L. W.; Near, R. D.; Boyuk, D. S.; Filler, M. A. Influence of Dielectric Anisotropy on the Absorption Properties of Localized Surface Plasmon Resonances Embedded in Si Nanowires. *J. Phys. Chem. C* **2014**, *118*, 5494−5500.
(32) Chou, L. W.; Shin, N.; Sivaram, S. V.; Filler, M. A. Tunable Mid-Infrared Localized Surface Plasmon Resonances in Silicon Nanowires. *J. Am. Chem. Soc.* **2012**, *134*, 16155−16158.
(33) Chou, L. W.; Filler, M. A. Engineering Multimodal Localized Surface Plasmon Resonances in Silicon Nanowires. *Angew. Chem., Int. Ed.* **2013**, *52*, 8079−8083.
(34) Chou, L. W.; Boyuk, D. S.; Filler, M. A. Optically Abrupt Localized Surface Plasmon Resonances in Si Nanowires by Mitigation of Carrier Density Gradients. *ACS Nano* **2015**, *9*, 1250−1256.
(35) Hsu, S. W.; Ngo, C.; Tao, A. R. Tunable and Directional Plasmonic Coupling within Semiconductor Nanodisk Assemblies. *Nano Lett.* **2014**, *14*, 2372−2380.
(36) Knight, M. W.; Wu, Y. P.; Lassiter, J. B.; Nordlander, P.; Halas, N. J. Substrates Matter: Influence of an Adjacent Dielectric on an Individual Plasmonic Nanoparticle. *Nano Lett.* **2009**, *9*, 2188−2192.
(37) Wu, Y. Y.; Yang, P. D. Direct Observation of Vapor-Liquid-Solid Nanowire Growth. *J. Am. Chem. Soc.* **2001**, *123*, 3165−3166.
(38) Harmand, J. C.; Patriarche, G.; Pere-Laperne, N.; Merat-Combes, M. N.; Travers, L.; Glas, F. Analysis of Vapor-Liquid-Solid Mechanism in Au-Assisted GaAs Nanowire Growth. *Appl. Phys. Lett.* **2005**, *87*, 203101.
(39) Jain, P. K.; El-Sayed, M. A. Noble Metal Nanoparticle Pairs: Effect of Medium for Enhanced Nanosensing. *Nano Lett.* **2008**, *8*, 4347−4352.
(40) Maier, S. A.; Brongersma, M. L.; Kik, P. G.; Atwater, H. A. Observation of near-Field Coupling in Metal Nanoparticle Chains Using Far-Field Polarization Spectroscopy. *Phys. Rev. B: Condens. Matter Mater. Phys.* **2002**, *65*, 193408.

DOI: 10.1021/acsphotonics.5b00581
ACS Photonics 2016, 3, 184−189

(41) Maier, S. A.; Kik, P. G.; Atwater, H. A.; Meltzer, S.; Harel, E.; Koel, B. E.; Requicha, A. A. G. Local Detection of Electromagnetic Energy Transport Below the Diffraction Limit in Metal Nanoparticle Plasmon Waveguides. *Nat. Mater.* **2003**, *2*, 229−232.
(42) Bjork, M. T.; Ohlsson, B. J.; Sass, T.; Persson, A. I.; Thelander, C.; Magnusson, M. H.; Deppert, K.; Wallenberg, L. R.; Samuelson, L. One-Dimensional Heterostructures in Semiconductor Nanowhiskers. *Appl. Phys. Lett.* **2002**, *80*, 1058−1060.
(43) Verheijen, M. A.; Immink, G.; De Smet, T.; Borgstrom, M. T.; Bakkers, E. P. A. M. Growth Kinetics of Heterostructured GaP-GaAs Nanowires. *J. Am. Chem. Soc.* **2006**, *128*, 1353−1359.
(44) Wen, C. Y.; Reuter, M. C.; Bruley, J.; Tersoff, J.; Kodambaka, S.; Stach, E. A.; Ross, F. M. Formation of Compositionally Abrupt Axial Heterojunctions in Silicon-Germanium Nanowires. *Science* **2009**, *326*, 1247−1250.
(45) Panciera, F.; Chou, Y. C.; Reuter, M. C.; Zakharov, D.; Stach, E. A.; Hofmann, S.; Ross, F. M. Synthesis of Nanostructures in Nanowires Using Sequential Catalyst Reactions. *Nat. Mater.* **2015**, *14*, 820−825.
(46) Christesen, J. D.; Pinion, C. W.; Zhang, X.; Mcbride, J. R.; Cahoon, J. F. Encoding Abrupt and Uniform Dopant Profiles in Vapor-Liquid-Solid Nanowires by Suppressing the Reservoir Effect of the Liquid Catalyst. *ACS Nano* **2014**, *8*, 11790−11798.
(47) Shin, N.; Filler, M. A. Controlling Silicon Nanowire Growth Direction Via Surface Chemistry. *Nano Lett.* **2012**, *12*, 2865−2870.
(48) Chou, L. W.; Shin, N.; Sivaram, S. V.; Filler, M. A. Tunable Mid-Infrared Localized Surface Plasmon Resonances in Silicon Nanowires. *J. Am. Chem. Soc.* **2012**, *134*, 16155−16158.
(49) Palik, E. D.; Ghosh, G. *Handbook of Optical Constants of Solids*; Academic Press: San Diego, 1998.

DOI: 10.1021/acsphotonics.5b00581
ACS Photonics 2016, 3, 184−189